

Aluminium-bearing strunzite derived from jahnsite at the Hagendorf-Süd pegmatite, Germany

I. E. GREY^{1,*}, C. M. MACRAE¹, E. KECK² AND W. D. BIRCH³

¹ CSIRO Process Science and Engineering, Box 312 Clayton South, Victoria 3169, Australia

² Algunderweg 3, D – 02694 Etzenricht, Germany

³ Geosciences, Museum Victoria, GPO Box 666, Melbourne, Victoria 3001, Australia

[Received 15 May 2012; Accepted 23 July 2012; Associate Editor: Giancarlo Della Ventura]

ABSTRACT

Aluminium-bearing strunzite, $[Mn_{0.65}Fe_{0.26}Zn_{0.08}Mg_{0.01}]^{2+}[Fe_{1.50}Al_{0.50}]^{3+}(PO_4)_2(OH)_2 \cdot 6H_2O$, occurs as fibrous aggregates in a crystallographically oriented association with jahnsite on altered zwieselite samples from the phosphate pegmatite at Hagendorf Süd, Bavaria, Germany. Synchrotron X-ray data were collected from a 3 µm diameter fibre and refined in space group $P\bar{1}$ to $R_1 = 0.054$ for 1484 observed reflections. The refinement confirmed the results of chemical analyses which showed that one quarter of the trivalent iron in the strunzite crystals is replaced by aluminium. The paragenesis revealed by scanning electron microscopy, in combination with chemical analyses and a crystal-chemical comparison of the strunzite and jahnsite structures, are consistent with strunzite being formed from jahnsite by selective leaching of (100) metal–phosphate layers containing large divalent Ca and Mn atoms.

KEYWORDS: Al-bearing strunzite, strunzite paragenesis, strunzite structure refinement, Hagendorf Süd secondary phosphates.

Introduction

STRUNZITE, ideally $Mn^{2+}Fe^{3+}(PO_4)_2(OH)_2 \cdot 6H_2O$, is a relatively rare secondary phosphate mineral found in altered granitic pegmatites (Moore, 1965; Viana and Prado, 2007; Dill *et al.*, 2008). It is a late-stage product in the supergene alteration of primary phosphate minerals such as triphyllite, zwieselite and apatite via intermediate phosphates including rockbridgeite, mitridatite, vivianite, whitmoreite and jahnsite (Mücke, 1981; Keller and Von Knorring, 1989; Dill *et al.*, 2008).

The presence of Al from the breakdown of aluminosilicates in contact with solutions rich in phosphate is a common feature of secondary pegmatite phosphate alteration (Franolet, 1980; Keller and von Knorring, 1989; Dill *et al.*, 2008).

The feldspar pegmatite at Hagendorf Süd, Bavaria, contains a large number of secondary Al-phosphates including eosporite, kingsmountite, paravauxite, fluellite, moromite, variscite, scorzalite, kastningite, nordgauite, whiteite and wavellite as well as Al-bearing secondary Fe–Mn phosphates including keckite, rockbridgeite and jahnsite (Mücke, 1981; Dill *et al.*, 2008; Grey *et al.*, 2010; Birch *et al.*, 2011). Strunzite is relatively widespread at Hagendorf Süd, and has been found (by E.K.) between the 45 and 84 m levels in the Cornelia mine open cut. It is particularly common between 60 and 67 m.

Dill *et al.* (2008) listed “Al-strunzite” as one of the phosphate minerals from the Hagendorf pegmatite province, but provided no details of its composition or occurrence. A few occurrences of fibrous Al-bearing strunzite in close association with Al-bearing jahnsite have been found in a continuing study of secondary phosphate minerals from the Cornelia mine open cut (Grey *et al.*,

* E-mail: ian.grey@csiro.au
DOI: 10.1180/minmag.2012.076.5.08

2010; Birch *et al.*, 2011). We have characterized both minerals by electron microprobe analysis and refined the structure of the strunzite from single-crystal synchrotron X-ray diffraction data. We report here the results of these studies together with an analysis of the crystal-chemical relationships between the two minerals, which provides evidence for formation of the strunzite by crystallographically controlled leaching of the jahnsite.

Experimental

Hand specimens containing strunzite associated with jahnsite on altered zwieselite were collected by one of us (E.K.) from the 67 m level of the Cornelia mine open cut. The strunzite occurs as sheaves of ultrathin white to yellowish fibres; the jahnsite occurs as transparent tabular crystals which are commonly corroded. Samples were mounted in epoxy blocks, polished and carbon-coated for scanning electron microscopy and electron microprobe (EMP) analyses by wavelength dispersive spectrometry on a JEOL JXA 8500F Hyperprobe operating at an accelerating voltage of 12 kV and a beam current of 11 nA. The beam was defocussed to a 1 µm spot size. The analytical standards used were CaSiO₃ for Ca; AlPO₄ for Al; P; MgAl₂O₄ for Mg; hematite for Fe; MnSiO₃ for Mn; ZnS for Zn and albite for Na. The EMP results are given in Table 1. All EMP data were corrected using a $\varphi(pz)$ matrix correction (Armstrong, 1988).

A needle-shaped crystal of strunzite, 80 µm long and ~3 µm in diameter, was used for X-ray data collection on the macromolecular beam line MX2 at the Australian Synchrotron. Data were

collected at room temperature using an ADSC Quantum 315r detector and monochromatic radiation with a wavelength of 0.71000 Å. A φ scan was employed with frame widths of 2° and a counting time per frame of 2 s. The intensity datasets were processed to produce data files which were analysed in WinGX (Farrugia, 1999). The refinement was made using SHELXL-97 (Sheldrick, 2008).

The published atom coordinates and metal atom site assignments for strunzite (Fanfani *et al.*, 1978) were used as the initial model for refinement in space group $P\bar{1}$. The scattering curve for Mn was used for the Mn site, which also contains minor Fe, Mg and Zn. Refinement with isotropic displacement parameters, and with refinement of Al/Fe occupancy in the two independent trivalent Fe sites converged to $R_1 = 0.08$. Hydrogen atoms associated with hydroxyl and water groups were located in difference-Fourier maps. They were refined with soft restraints on the O–H and H–H distances of O–H = 0.80(4) Å and H–H = 1.25(8) Å. These restrained O–H distances are consistent with distances reported in previous X-ray refinements (e.g. Harte *et al.*, 2005). A common isotropic displacement parameter was refined for the hydrogen atoms. The final refinement, incorporating anisotropic displacement parameters for all non-H atoms, converged to $R_1 = 0.054$ for 1481 observed reflections with $F > 4\sigma(F)$. Further details of the refinement are summarized in Table 2. Refined atom coordinates and equivalent isotropic displacement parameters are reported in Table 3. Tables of anisotropic displacement parameters and observed and calculated structure factors have been deposited with the Principal

TABLE 1. Electron microprobe analyses of Al-bearing strunzite and jahnsite from Hagendorf Süd.

	Strunzite (9 analyses) Range (wt.%)	Mean (wt.%)	Jahnsite (7 analyses) Range (wt.%)	Mean (wt.%)
CaO	0–0.12	0.05	5.22–6.39	5.48
Na ₂ O	0–0.02	0.01	0.11–0.24	0.15
MnO	9.01–10.90	10.29	14.09–19.25	17.20
Fe ₂ O ₃	29.19–34.48	31.25	16.87–21.02	18.97
Al ₂ O ₃	5.39–6.25	5.74	1.71–3.93	2.91
MgO	0–0.09	0.09	0.75–1.17	0.92
ZnO	1.33–1.61	1.39	1.67–2.40	2.07
P ₂ O ₅	29.90–32.61	31.07	31.69–33.96	32.69
Total	76.60–84.30	79.89	78.07–83.35	80.39

TABLE 2. Data collection and structure refinement details for Al-bearing strunzite.

Crystal data	
Unit cell: a , b , c (Å)	10.277(1), 9.826(1), 7.205(1)
Unit cell: α , β , γ (°)	90.077(4), 98.865(4), 118.442(4)
Volume (Å ³)	629.8(1)
Z	2
Space group	$P\bar{1}$
Calculated density (g cm ⁻³)	2.54
Formula from refinement	$MnFe_{1.44}Al_{0.56}(PO_4)_2(OH)_2 \cdot 6H_2O$
Formula weight	970.0
Data collection	
Temperature (K)	293
Wavelength (Å)	0.7100
Crystal size (mm)	0.003 diameter \times 0.08 long
Collection mode	φ scan, 360°, $\Delta\Phi = 0.02^\circ$
Count time per frame (s)	2
$2\theta_{max}$ (°)	50
No. of unique reflections	2024
No. of reflections, $I > 2\sigma(I)$	1484
Absorption coefficient (mm ⁻¹)	3.19
Refinement	
Data/restraints/parameters	2024/20/235
Goodness-of-fit	0.892
Final R indices ($F > 4\sigma(F)$)	$R_1 = 0.054$, $wR_2 = 0.128$
Final R indices (all data)	$R_1 = 0.078$, $wR_2 = 0.145$
Largest diff. peak and hole (e Å ⁻³)	-0.68, +1.06

Editors and can be downloaded from http://www.minersoc.org/pages/e_journals/dep_mat_mm.html.

Results and discussion

Electron probe microanalysis and paragenesis

The EMP analyses of the strunzite and associated jahnsite crystals are reported in Table 1. Both phases show relatively high compositional homogeneity between different regions, with no strong inter-element correlations. Weak positive correlations between the Mn, Al and Fe analyses appear to reflect variable analytical totals, possibly due to varying water loss resulting from heating by the electron beam. The jahnsite is Al-bearing and its composition is close to that we have previously reported for jahnsite-(CaMnMn) in contact with zwieselite-triplite and with nordgauite in samples from the Cornelia mine open cut (Grey *et al.*, 2010). Mücke (1981) reported Al-bearing keckite, $CaMn_2(Fe,Al)_3(OH)_3(PO_4)_4 \cdot xH_2O$, associated with strunzite in altered zwieselite

secondary phosphate assemblages at Hagendorf. According to recent studies, however, keckite can be mistaken for jahnsite-(CaMnFe) or jahnsite-(CaMnMn) (Hochleitner and Fehr, 2010; Kampf *et al.*, 2008).

The strunzite analyses are similar to those reported by Frondel (1958), but with one quarter of the Fe replaced by Al, giving a formula $Mn_{0.65}Fe_{1.76}Al_{0.50}Zn_{0.08}Mg_{0.01}(PO_4)_2(OH) \cdot 6H_2O$. For comparison, the ideal strunzite formula is $MnFe_2(PO_4)_2(OH) \cdot 6H_2O$, and the formula from the structure refinement is $MnFe_{1.44}Al_{0.56}(PO_4)_2(OH) \cdot 6H_2O$. The analyses reported in Table 1 show that strunzite and jahnsite have similar Fe/Al ratios but the amount of these trivalent elements in strunzite is about double that in jahnsite. We propose that this chemical relationship is due to the strunzite being formed from jahnsite by selective leaching of divalent phosphate components, thereby enriching the trivalent element concentrations.

This type of paragenesis is supported by the spatial relationship between the two phases,

TABLE 3. Atom coordinates ($\times 10^4$) and equivalent isotropic displacement parameters ($\text{\AA}^2 \times 10^3$) for Al-bearing strunzite; U_{eq} is one third of the trace of the orthogonalized U_{ij} tensor.

	x/a	y/b	z/c	$U_{\text{eq}} (\text{\AA}^2)$
Mn	5002(1)	3289(1)	2497(2)	18(1)
Fe(1)*	9694(1)	2439(1)	1384(2)	12(1)
Fe(2)*	301(1)	7741(1)	3618(2)	13(1)
P(1)	8132(2)	4666(2)	584(3)	12(1)
P(2)	1869(2)	1527(2)	4415(3)	13(1)
O(1)	6474(6)	4022(7)	635(8)	25(1)
O(2)	8417(6)	3304(6)	214(8)	23(1)
O(3)	9097(6)	5559(6)	2471(7)	16(1)
O(4)	8496(6)	5706(6)	8944(7)	19(1)
O(5)	901(6)	1456(6)	2512(7)	16(1)
O(6)	1564(6)	-122(6)	4777(8)	21(1)
O(7)	3515(6)	2515(6)	4379(8)	24(1)
O(8)	1529(6)	2226(6)	6036(8)	19(1)
OH1	9615(6)	3094(6)	3917(8)	19(1)
OH2	384(6)	8474(6)	1084(8)	20(1)
Ow1	3087(7)	2407(7)	120(9)	27(1)
Ow2	6922(7)	4330(6)	4882(9)	25(1)
Ow3	4997(7)	5511(7)	2502(9)	29(1)
Ow4	5032(11)	1024(9)	2504(15)	59(2)
Ow5	2317(7)	7766(7)	3361(9)	27(1)
Ow6	-2319(7)	456(6)	1652(9)	24(1)
HOH1	9460(120)	3800(90)	3840(150)	39(8)
HOH2	360(120)	9270(70)	1220(150)	39(8)
H1A	3110(120)	2770(110)	-910(80)	39(8)
H1B	2500(100)	2500(120)	570(130)	39(8)
H2A	6770(110)	4720(110)	5770(110)	39(8)
H2B	7680(70)	4900(90)	4590(140)	39(8)
H3A	5540(90)	6240(80)	3290(110)	39(8)
H3B	4260(70)	5070(100)	2950(140)	39(8)
H4A	4920(120)	1110(120)	1400(60)	39(8)
H4B	4290(80)	380(100)	2800(140)	39(8)
H5A	2130(120)	7360(110)	2290(70)	39(8)
H5B	2420(120)	7140(100)	4000(110)	39(8)
H6A	-1950(120)	290(110)	2600(80)	39(8)
H6B	-2450(120)	-270(90)	970(110)	39(8)

* Refined site occupancies for Fe(1) and Fe(2) are both 0.72(1)Fe + 0.28(1)Al.

which is shown in the photomicrographs in Fig. 1. The tabular jahnsite crystals are heavily corroded, and Fig. 1a shows the transformation of the ends of the crystals into fibrous strunzite. The axes of the strunzite fibres are parallel to the long dimension of the jahnsite crystal. Precession single-crystal XRD studies on excavated grains showed that the fibre axis of the strunzite, c , and the axis corresponding to the long dimension of the jahnsite crystals, b , are crystallographically equivalent 7.2 Å axes, corresponding to the repeat distance of chains of corner-connected Fe-centred

octahedra that are common to both minerals. An advanced stage of the breakdown of jahnsite to fibrous strunzite is shown in Fig. 1b. The transformation of jahnsite into strunzite is explained in the following sections by comparing their crystal structures.

Strunzite crystal structure

The only published crystal-structure analysis of strunzite is due to Fanfani *et al.* (1978). They studied fibrous strunzite from the Big Chief mine,

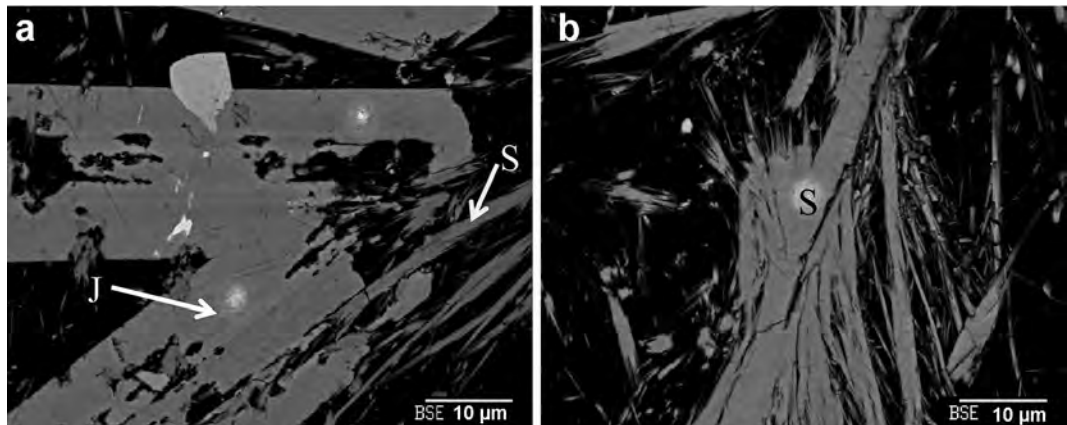
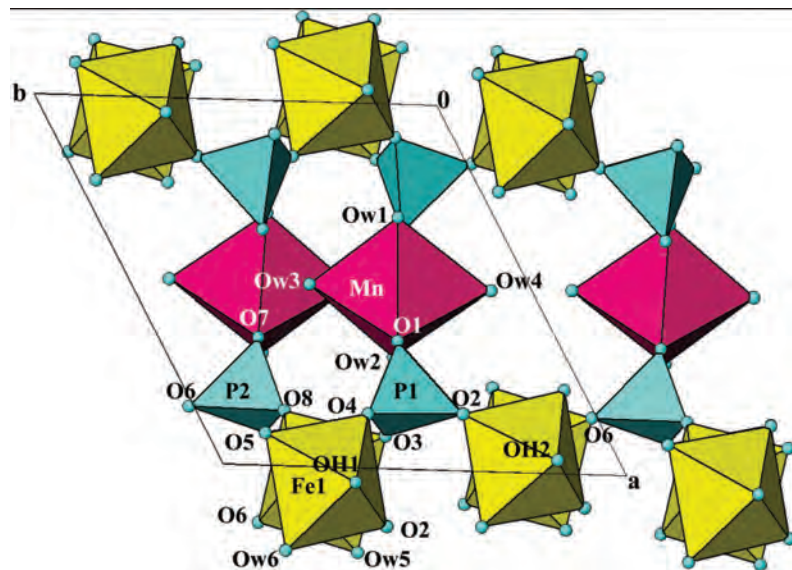


FIG. 1. (a) An SEM image showing jahnsite (J) associated with Al-bearing strunzite (S). (b) An SEM image showing the development of strunzite fibres from jahnsite.

Dakota, and noted problems due to the poor quality of the data. Anisotropic refinement gave non-positive displacement parameters for some oxygen atoms, and the H atoms were not located. Our synchrotron analysis produced good quality data, albeit of very low intensity due to the tiny crystal diameter, and anisotropic refinement gave reasonable displacement parameters for all non-H atoms. In addition the H atoms were located, allowing the H-bonding scheme to be determined.

In their review of the crystal chemistry of phosphate minerals, Huminicki and Hawthorne (2002) included strunzite in the subgroup of infinite sheets of PO_4 tetrahedra and $\text{M}\Phi_6$ octahedra ($\Phi = \text{O}, \text{OH}, \text{H}_2\text{O}, \text{F}$). The sheets consist of 7.2 Å chains of Fe-centred octahedra, *trans*-corner-linked through OH along [001], and interconnected via corner-sharing with PO_4 tetrahedra along [010] to form (100) sheets. The sheets are interconnected along [100] by corner-



sharing of the tetrahedra with $\text{MnO}_2(\text{H}_2\text{O})_4$ octahedra, as illustrated in Fig. 2. The Fe-centred octahedra have the composition $\text{FeO}_3(\text{OH})_2(\text{H}_2\text{O})$. The occupancy of the Fe sites obtained from the structure refinement is 0.72(1) Fe + 0.28(1) Al. This compares well with the results from the microprobe analyses, which produce a formula $[\text{Mn}_{0.65}\text{Fe}_{0.26}\text{Zn}_{0.08}\text{Mg}_{0.01}]^{2+}[\text{Fe}_{1.50}\text{Al}_{0.50}]^{3+}(\text{PO}_4)_2(\text{OH})_2\cdot6\text{H}_2\text{O}$, after appropriate assignment of the elements into the M^{2+} and M^{3+} sites. In particular, $0.75\text{Fe}^{3+} + 0.25\text{Al}^{3+}$ are present in the Fe sites. The partial occupation of the Fe sites by Al results in shorter M–O bonds (with a mean distance of 1.987(6) Å) than those reported for strunzite (2.01(1) Å), although the difference is barely significant within the associated errors. In general, the bond lengths in Table 4 closely match those reported by Fanfani *et al.* (1978). The long M–Ow distances for both the Fe and Mn sites (Table 4) are notable.

Hydrogen bonds with O–O distances <3 Å are listed in Table 5. Most of the assignments agree with those proposed by Fanfani *et al.* (1978) from bond-valence considerations. The majority of the stronger H-bonds lie close to (100) planes, as shown in Fig. 3. The strongest H-bonds are between Ow and O of adjacent intrachain octahedra. In jahnsite and related minerals such

pairs of anions (Ow6 and O6, Ow5 and O2) form the edges of PO_4 tetrahedra, giving four bridging intrachain tetrahedra per octahedron, compared to only two in strunzite.

Jahnsite to strunzite transformation

The general formula for jahnsite-group minerals can be written $\text{XM}(1)\text{M}(2)_2\text{Fe}_2(\text{PO}_4)_4(\text{OH})_2\cdot8\text{H}_2\text{O}$. The dominant elements in the first three sites are added as a suffix to produce species names of the form jahnsite-($\text{XM}(1)\text{M}(2)$) (Moore and Ito, 1978). Generally these elements are divalent and are listed in order of decreasing ionic radius. Using this nomenclature, the original jahnsite described by Moore (1974) is jahnsite-(CaMnMg). Recently, a new variation involving monovalent Na in the X site and trivalent Fe in M(1) site has been reported (Kampf *et al.*, 2008).

The structure of jahnsite was first determined by Moore and Araki (1974). A view of the structure in projection along the 7.2 Å *b* axis is shown in Fig. 4*a*. It consists of [010] chains of *trans*-corner-connected Fe-centred octahedra, $\text{FeO}_4(\text{OH})_2$, that are decorated by bridging PO_4 tetrahedra to give columns of composition $\text{Fe}(\text{PO}_4)_2(\text{OH})$. The columns connect along [100] with [010] chains of edge-shared XO_6 and $\text{M}(1)\text{O}_6$ octahedra to form (001) sheets. These

TABLE 4. Selected bond lengths (Å) for Al-bearing strunzite.

Mn–O(1)	2.049(6)		
Mn–O(7)	2.071(6)		
Mn–Ow3	2.185(6)		
Mn–Ow1	2.211(6)		
Mn–Ow2	2.219(6)		
Mn–Ow4	2.240(7)		
<Mn–O>	2.162		
Fe(1)–O(4)	1.936(5)	Fe(2)–O(8)	1.951(5)
Fe(1)–OH1	1.961(5)	Fe(2)–O(6)	1.964(5)
Fe(1)–OH2	1.964(5)	Fe(2)–OH2	1.963(6)
Fe(1)–O(2)	1.968(5)	Fe(2)–OH1	1.964(6)
Fe(1)–O(5)	1.992(5)	Fe(2)–O(3)	1.991(5)
Fe(1)–Ow6	2.097(6)	Fe(2)–Ow5	2.097(6)
<Fe(1)–O>	1.986	<Fe(2)–O>	1.988
P(1)–O(1)	1.516(6)	P(2)–O(7)	1.501(6)
P(1)–O(3)	1.534(5)	P(2)–O(8)	1.520(6)
P(1)–O(2)	1.532(5)	P(2)–O(6)	1.528(5)
P(1)–O(4)	1.534(6)	P(2)–O(5)	1.545(5)
<P(1)–O>	1.529	<P(2)–O>	1.524

TABLE 5. Hydrogen bond lengths and angles (\AA and $^\circ$) for Al-bearing strunzite.

D-H…A	D-H	H…A	D…A	$\angle(\text{DHA})$
OH1—HOH1…O(3)	0.79(4)	2.14(6)	2.880(7)	156(10)
OH2—HOH2…O(5) ⁱ	0.80(4)	2.12(6)	2.875(7)	158(10)
Ow1—H1B…O(5)	0.77(4)	2.19(6)	2.844(9)	142(9)
Ow1—H1A…Ow3 ⁱⁱ	0.82(4)	2.35(8)	2.992(10)	135(9)
Ow2—H2B…O(3)	0.78(4)	2.16(6)	2.846(9)	148(10)
Ow2—H2A…Ow3 ⁱⁱⁱ	0.82(4)	2.28(6)	2.986(10)	144(9)
Ow3—H3A…O(7) ⁱⁱⁱ	0.82(4)	1.90(5)	2.693(8)	162(10)
Ow3—H3B…Ow2 ⁱⁱⁱ	0.79(4)	2.35(7)	2.985(10)	138(9)
Ow5—H5A…O(2) ⁱⁱ	0.82(4)	1.82(4)	2.636(8)	170(10)
Ow5—H5B…Ow2 ⁱⁱⁱ	0.81(4)	1.98(5)	2.773(8)	164(11)
Ow6—H6A…O(6) ^{iv}	0.79(4)	1.89(5)	2.638(8)	158(10)
Ow6—H6B…Ow1 ^v	0.81(4)	2.00(5)	2.781(8)	163(10)

Symmetry codes: (i) $x, y+1, z$; (ii) $-x+1, -y+1, -z$; (iii) $-x+1, -y+1, -z+1$; (iv) $-x, -y, -z+1$; (v) $-x, -y, -z$.

sheets connect along [001] by corner-sharing of the PO_4 tetrahedra with $\text{M}(2)\text{O}_2(\text{H}_2\text{O})_4$ octahedra.

An alternative description of the structure in terms of (100) polyhedral sheets emphasizes the separation of large weakly bonded X and M(1) atoms from small tightly bonded trivalent Fe atoms in alternate (100) layers. The two types of layers are shown in Fig. 4a. Removal of the planes containing X and M(1) and associated PO_4

and $\text{M}(2)\Phi_6$ polyhedra gives the residual polyhedral layers shown in Fig. 4b. Breaking one quarter of the intrachain bridging PO_4 links (which are replaced by H_2O) and then connecting the layers by corner-sharing between PO_4 and $\text{Fe}\Phi_6$ (indicated by the arrows in Fig. 4b) generates the strunzite structure (cf. Fig. 2). These structural considerations suggest that strunzite could form from jahnsite by selective

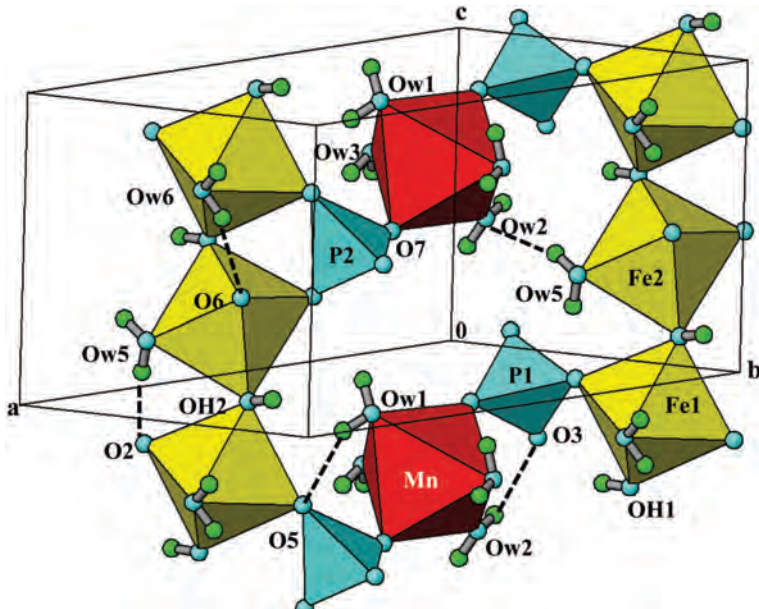


FIG. 3. An (010) slice through the strunzite structure, showing the H-bonding arrangement.

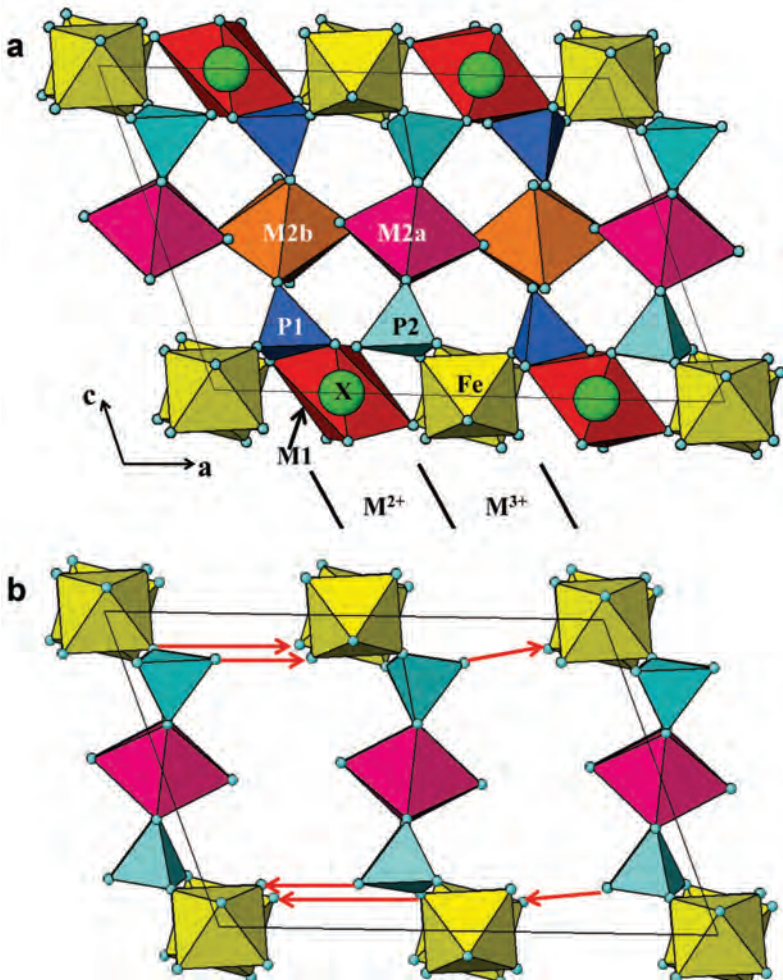
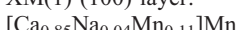


FIG. 4. (a) Projection of jahnsite structure along [010]. (b) Jahnite after the removal of (010) layers of XM(1)P(1)M(2b) polyhedra. The arrows show the interlayer corner-sharing connections that are required to generate the strunzite structure.

leaching of (100) layers containing the large divalent X and M(1) atoms.

Supporting evidence for this mechanism is provided by the EMP analyses of the two coexisting phases. The jahnsite formula, calculated from the results in Table 1 is $[Ca_{0.85}Na_{0.04}Mn_{0.11}]Mn[Mn_{1.02}Fe_{0.56}Zn_{0.22}Mg_{0.20}][Fe_{1.50}Al_{0.50}](PO_4)_4(OH)_2 \cdot 8H_2O$, where the atoms are assigned to the X, M(1), M(2) and Fe/Al sites in order of decreasing size. The M(2) and PO₄ sites in alternate (100) layers are crystallographically independent, so the composition can be separated into two layers as follows:

XM(1) (100) layer:



Fe³⁺-containing (100) layer:



For comparison the Al-bearing strunzite formula from the EMP analyses in Table 1 is



There is a close match between the Al-bearing strunzite formula and that of the second jahnsite

(100) layer, particularly in the level of Al substitution in the Fe sites, which is consistent with the strunzite being derived from the jahnsite by leaching of the XM(1)-containing (100) layers. An extension of this type of mechanism to the leaching of whiteite, the Al analogue of jahnsite, would predict the formation of an Al-dominant strunzite. Whiteite-(CaMnMn) is present in secondary phosphate assemblages at Hagendorf Süd (Chernyatieva *et al.*, 2010; Grey *et al.*, 2010), but despite extensive investigation we have not yet located any associated Al-dominant strunzite-type phase.

Conclusions

Aluminium-bearing strunzite and jahnsite are found in close association at the 67 m level of the Cornelia mine open cut at Hagendorf Süd. Their crystallographically oriented spatial relationship and respective morphologies (corroded tabular jahnsite grading into fibrous strunzite) are consistent with strunzite being derived from jahnsite by supergene alteration reactions. A comparative study of the two minerals reveals a close structural relationship: the jahnsite structure contains (100) layers with a strunzite-type structure and composition, alternating with (100) layers containing larger divalent atoms. There is a close chemical match between the composition of the strunzite-like layers in jahnsite and the associated strunzite crystals. This leads to a proposed paragenetic mechanism involving the selective leaching of the (100) layers containing large divalent metal atoms, followed by linkage of the residual strunzite-like layers. If such a mechanism was also applicable to whiteite it would produce a new Al-dominant analogue of strunzite.

Acknowledgements

Part of the study was conducted on the macromolecular crystallography beamline at the Australian Synchrotron, Clayton, Victoria. We thank Drs Rachel Williamson, Christine Gee and Tom Caraduc-Davies at the beamline for assistance with the synchrotron data collection.

References

- Armstrong, J.T. (1988) Quantitative analysis of silicate and oxide materials: comparison of Monte Carlo, ZAF and $\phi(\rho_z)$ procedures. Pp. 239–246 in: *Microbeam Analysis* (D.E. Newbury, editor). San Francisco Press, San Francisco, California, USA.
- Birch, W.D., Grey, I.E., Mills, S.J., Pring, A., Wilson, N.C. and Keck, E. (2011) Nordgauite, $MnAl_2(PO_4)_2(F,OH)_2 \cdot 5.5H_2O$, a new mineral from the Hagendorf Süd pegmatite, Bavaria, Germany: description and crystal structure. *Mineralogical Magazine*, **75**, 269–278.
- Chernyatieva, A.P., Krivovichev, S.V., Yakovenchuk, V.N. and Pakhomovsky, Y.A. (2010) Crystal chemistry of a new CaMnMn-dominant member of the whiteite group. In Abstracts, IMA2010, 20th General Meeting of the International Mineralogical Association, 21–27 August, 2010, Budapest, Hungary. *Acta Mineralogica-Petrographica Abstract Series*, **6**, 716. Department of Mineralogy, Geochemistry and Petrology, University of Szeged, Hungary.
- Dill, H.G., Weber, B., Gerdes, A. and Melcher, F. (2008) The Fe-Mn phosphate aplite ‘Silbergrube’ near Waidhaus, Germany: epithermal phosphate mineralization in the Hagendorf-Pleystein province. *Mineralogical Magazine*, **72**, 1119–1144.
- Fanfani, L., Tomassini, M., Zanazzi, P.F. and Zanzari, A.R. (1978) The crystal structure of strunzite, a contribution to the crystal chemistry of basic ferric-manganous hydrated phosphates. *Tschermaks Mineralogische und Petrographische Mitteilungen*, **25**, 77–87.
- Farrugia, L.J. (1999) WinGX suite for small-molecule single-crystal crystallography. *Journal of Applied Crystallography*, **32**, 837–838.
- Frondel, C. (1958) Strunzite, a new mineral. *Naturwissenschaften*, **45**, 37–38.
- Fransolet, A.-M. (1980) The eosphorite–childrenite series associated with the Li-Mn-Fe phosphate minerals from the Buranga pegmatite, Rwanda. *Mineralogical Magazine*, **43**, 1015–1023.
- Grey, I.E., Mumme, W.G., Neville, S.M., Wilson, N.C. and Birch, W.D. (2010) Jahnsite–whiteite solid solutions and associated minerals in the phosphate pegmatite at Hagendorf-Süd, Bavaria, Germany. *Mineralogical Magazine*, **74**, 969–978.
- Harte, S.M., Parkin, A., Goeta, A. and Wilson, C.C. (2005) Using neutrons and X-rays to study the effect of temperature on the short hydrogen bond in potassium hydrogen phthalate. *Journal of Molecular Structure*, **741**, 93–96.
- Hochleitner, R. and Fehr, K. (2010) The keckite problem and its bearing on the crystal chemistry of the jahnsite group: Mössbauer and electron-microprobe studies. *The Canadian Mineralogist*, **48**, 1445–1453.
- Huminicki, D.M.C. and Hawthorne, F.C. (2002) The crystal chemistry of the phosphate minerals. Pp. 123–253 in: *Phosphates: Geochemical and Materials Importance* (M.J.

- Kohn, J. Rakovan and J.M. Hughes, editors). Reviews in Mineralogy & Geochemistry, **48**. Mineralogical Society of America, Washington DC and the Geochemical Society, St Louis, Missouri, USA.
- Kampf, A.R., Steele, I.M. and Loomis, T.A. (2008) Jahnsite-(NaFeMg), a new mineral from the Tip Top mine, Custer County, South Dakota: description and crystal structure. *American Mineralogist*, **93**, 940–945.
- Keller, P. and von Knorring, O. (1989) Pegmatites at the Okatjimukuju farm, Karibib, Namibia. Part I: phosphate mineral associations of the Clementine II pegmatite. *European Journal of Mineralogy*, **1**, 567–593.
- Moore, P.B. (1965) Hühnerkobelite crystals from the Palermo No. 1 pegmatite, North Groton, New Hampshire. *American Mineralogist*, **50**, 713–717.
- Moore, P.B. (1974) I. Jahnsite, segelerite and robertsite, three new transition metal phosphate species. II. Redefinition of overite, an isotype of segelerite. III. Isotypy of robertsite, mitridatite and arseniosiderite. *American Mineralogist*, **59**, 48–59.
- Moore, P.B. and Araki, T. (1974) Jahnsite, $\text{CaMn}^{2+}\text{Mg}_2(\text{H}_2\text{O})_8\text{Fe}^{3+}(\text{OH})_2[\text{PO}_4]_4$: a novel stereoisomerism of ligands about octahedral corner-chains. *American Mineralogist*, **59**, 964–973.
- Moore, P.B. and Ito, J. (1978) I. Whiteite, a new species, and a proposed nomenclature for the jahnsite–whiteite complex series. II. New data on xanthoxenite. III. Salmonsite discredited. *Mineralogical Magazine*, **42**, 309–323.
- Mücke, A. (1981) The paragenesis of the phosphate minerals of the Hagendorf pegmatite – a general view. *Chemie der Erde*, **40**, 217–234.
- Sheldrick, G.M. (1997) *SHELXL-97, a program for crystal structure refinement*. University of Göttingen, Göttingen, Germany.
- Viana, R.R. and Prado, R.J. (2007). Mineralogical and chemical characterization of vivianite occurrence in pegmatites from the Eastern Brazilian pegmatite province. Unpaginated abstract in: *Granitic Pegmatites: the State of the Art* (T. Martins and R. Vieira, editors). Memórias 8. Department of Geology, University of Porto, Porto, Portugal.

Table D1. Anisotropic displacement parameters ($\text{Å}^2 \times 10^3$) for Al-bearing strunzite.

The anisotropic displacement factor exponent takes the form:
 $-2 \pi^2 [h^2 a^{*2} U_{11} + \dots + 2 h k a^* b^* U_{12}]$

	U_{11}	U_{22}	U_{33}	U_{23}	U_{13}	U_{12}
Mn	15(1)	16(1)	24(1)	-1(1)	1(1)	9(1)
Fe(1)	13(1)	9(1)	14(1)	-3(1)	-4(1)	8(1)
Fe(2)	15(1)	8(1)	16(1)	-4(1)	-4(1)	8(1)
P(1)	12(1)	8(1)	17(1)	-2(1)	-1(1)	6(1)
P(2)	13(1)	10(1)	16(1)	-1(1)	-3(1)	7(1)
O(1)	16(3)	35(3)	20(3)	0(2)	0(2)	9(3)
O(2)	31(3)	20(3)	21(3)	-7(2)	-10(2)	19(3)
O(3)	21(3)	15(2)	16(3)	-2(2)	0(2)	12(2)
O(4)	24(3)	15(3)	15(3)	1(2)	-3(2)	10(2)
O(5)	14(3)	15(2)	19(3)	-2(2)	-5(2)	9(2)
O(6)	29(3)	19(3)	19(3)	1(2)	-5(2)	19(2)
O(7)	16(3)	29(3)	20(3)	-4(2)	-1(2)	6(3)
O(8)	12(3)	17(3)	25(3)	-4(2)	-4(2)	7(2)
OH1	25(3)	19(3)	20(3)	-3(2)	-4(2)	18(2)
OH2	29(3)	10(2)	23(3)	-5(2)	-6(2)	13(2)
Ow1	26(3)	30(3)	30(4)	-4(3)	1(3)	20(3)
Ow2	21(3)	18(3)	30(4)	-1(2)	0(3)	7(2)
Ow3	35(4)	20(3)	28(4)	-5(3)	-7(3)	14(3)
Ow4	68(6)	28(4)	87(7)	0(4)	7(5)	29(4)
Ow	30(3)	30(3)	28(4)	-3(3)	-2(3)	22(3)
Ow	28(3)	18(3)	22(4)	-3(2)	-5(3)	12(3)

```

data_strunzwat_anis

_audit_creation_method           SHELXL-97
_chemical_name_systematic
;
?
;
_chemical_name_common            strunzite
_chemical_melting_point          ?
_chemical_formula_moiety         ?
_chemical_formula_sum
'H28 Al Fe3.52 Mg0.02 Mn1.30 O32 P4 Zn0.16'
_chemical_formula_weight          970.04

loop_
_atom_type_symbol
_atom_type_description
_atom_type_scat_dispersion_real
_atom_type_scat_dispersion_imag
_atom_type_scat_source
'O'   'O'   0.0106   0.0060
'International Tables Vol C Tables 4.2.6.8 and 6.1.1.4'
'H'   'H'   0.0000   0.0000
'International Tables Vol C Tables 4.2.6.8 and 6.1.1.4'
'Al'   'Al'   0.0645   0.0514
'International Tables Vol C Tables 4.2.6.8 and 6.1.1.4'
'P'   'P'   0.1023   0.0942
'International Tables Vol C Tables 4.2.6.8 and 6.1.1.4'
'Mn'   'Mn'   0.3368   0.7283
'International Tables Vol C Tables 4.2.6.8 and 6.1.1.4'
'Fe'   'Fe'   0.3463   0.8444
'International Tables Vol C Tables 4.2.6.8 and 6.1.1.4'
'Zn'   'Zn'   0.2839   1.4301
'International Tables Vol C Tables 4.2.6.8 and 6.1.1.4'
'Mg'   'Mg'   0.0486   0.0363
'International Tables Vol C Tables 4.2.6.8 and 6.1.1.4'

_symmetry_cell_setting          ?
_symmetry_space_group_name_H-M    ?

loop_
_symmetry_equiv_pos_as_xyz
'x, y, z'
'-x, -y, -z'

_cell_length_a                  10.2770(10)
_cell_length_b                  9.8260(10)
_cell_length_c                  7.2050(10)
_cell_angle_alpha                90.077(4)
_cell_angle_beta                 98.865(4)
_cell_angle_gamma                118.442(4)
_cell_volume                     629.77(12)
_cell_formula_units_Z            1
_cell_measurement_temperature    293(2)
_cell_measurement_reflns_used    ?
_cell_measurement_theta_min      ?
_cell_measurement_theta_max      ?

_exptl_crystal_description       fibre

```

```

_exptl_crystal_colour          ?
_exptl_crystal_size_max        0.08 mm
_exptl_crystal_size_mid         ?
_exptl_crystal_size_min        0.003 mm
_exptl_crystal_density_meas    ?
_exptl_crystal_density_diffrn  2.558
_exptl_crystal_density_method   'not measured'
_exptl_crystal_F_000           486
_exptl_absorpt_coefficient_mu  3.188
_exptl_absorpt_correction_type ?
_exptl_absorpt_correction_T_min ?
_exptl_absorpt_correction_T_max ?
_exptl_absorpt_process_details ?


_exptl_special_details
;
?
;

_diffrn_ambient_temperature     293(2)
_diffrn_radiation_wavelength    0.71000
_diffrn_radiation_type          Synchrotron
_diffrn_radiation_source
_diffrn_radiation_monochromator
_diffrn_measurement_device_type phi scan
_diffrn_measurement_method      ?
_diffrn_detector_area_resol_mean ?
_diffrn_standards_number        ?
_diffrn_standards_interval_count ?
_diffrn_standards_interval_time ?
_diffrn_standards_decay_%       ?
_diffrn_reflns_number           7372
_diffrn_reflns_av_R_equivalents 0.1706
_diffrn_reflns_av_sigmaI/netI   0.1307
_diffrn_reflns_limit_h_min      -12
_diffrn_reflns_limit_h_max      12
_diffrn_reflns_limit_k_min      -11
_diffrn_reflns_limit_k_max      11
_diffrn_reflns_limit_l_min      -8
_diffrn_reflns_limit_l_max      8
_diffrn_reflns_theta_min        2.29
_diffrn_reflns_theta_max        25.00
_reflns_number_total            2024
_reflns_number_gt               1484
_reflns_threshold_expression    >2sigma(I)

_computing_data_collection      ?
_computing_cell_refinement      ?
_computing_data_reduction       ?
_computing_structure_solution   ?
_computing_structure_refinement 'SHELXL-97 (Sheldrick, 1997)'
_computing_molecular_graphics   ?
_computing_publication_material ?


_refine_special_details
;
Refinement of F^2^ against ALL reflections. The weighted R-factor wR and
goodness of fit S are based on F^2^, conventional R-factors R are based
on F, with F set to zero for negative F^2^. The threshold expression of
F^2^ > 2sigma(F^2^) is used only for calculating R-factors(gt) etc. and is
not relevant to the choice of reflections for refinement. R-factors based

```

on F^2^ are statistically about twice as large as those based on F, and R-factors based on ALL data will be even larger.

;

_refine_ls_structure_factor_coef Fsqd
_refine_ls_matrix_type full
_refine_ls_weighting_scheme calc
_refine_ls_weighting_details 'calc w=1/[s^2^(Fo^2^)+(0.0600P)^2^+0.0000P] where P=(Fo^2^+2Fc^2^)/3'
_atom_sites_solution_primary direct
_atom_sites_solution_secondary difmap
_atom_sites_solution_hydrogens geom
_refine_ls_hydrogen_treatment mixed
_refine_ls_extinction_method none
_refine_ls_extinction_coeff ?
_refine_ls_number_reflns 2024
_refine_ls_number_parameters 235
_refine_ls_number_restraints 20
_refine_ls_R_factor_all 0.0785
_refine_ls_R_factor_gt 0.0544
_refine_ls_wR_factor_ref 0.1425
_refine_ls_wR_factor_gt 0.1281
_refine_ls_goodness_of_fit_ref 0.892
_refine_ls_restrained_S_all 0.888
_refine_ls_shift/su_max 0.322
_refine_ls_shift/su_mean 0.015

loop_

_atom_site_label
_atom_site_type_symbol
_atom_site_fract_x
_atom_site_fract_y
_atom_site_fract_z
_atom_site_U_iso_or_equiv
_atom_site_adp_type
_atom_site_occupancy
_atom_site_symmetry_multiplicity
_atom_site_calc_flag
_atom_site_refinement_flags
_atom_site_disorder_assembly
_atom_site_disorder_group

Mn1 Mn 0.50018(13) 0.32893(13) 0.24966(18) 0.0181(4) Uani 1 1 d . . .
Fe1 Fe 0.96937(13) 0.24395(13) 0.13836(17) 0.0117(5) Uani 0.723(12) 1 d P . .
Al1 Al 0.96937(13) 0.24395(13) 0.13836(17) 0.0117(5) Uani 0.277(12) 1 d P . .
Fe2 Fe 0.03012(14) 0.77407(13) 0.36181(18) 0.0130(5) Uani 0.716(11) 1 d P . .
Al2 Al 0.03012(14) 0.77407(13) 0.36181(18) 0.0130(5) Uani 0.284(11) 1 d P . .
P1 P 0.8132(2) 0.4666(2) 0.0584(3) 0.0124(5) Uani 1 1 d . . .
P2 P 0.1869(2) 0.1527(2) 0.4415(3) 0.0129(5) Uani 1 1 d . . .
O1 O 0.6474(6) 0.4022(7) 0.0635(8) 0.0249(13) Uani 1 1 d . . .
O2 O 0.8417(6) 0.3304(6) 0.0214(8) 0.0226(13) Uani 1 1 d . . .
O3 O 0.9097(6) 0.5559(6) 0.2471(7) 0.0164(12) Uani 1 1 d . . .
O4 O 0.8496(6) 0.5706(6) 0.8944(7) 0.0189(12) Uani 1 1 d . . .
O5 O 0.0901(6) 0.1456(6) 0.2512(7) 0.0164(12) Uani 1 1 d . . .
O6 O 0.1564(6) -0.0122(6) 0.4777(8) 0.0205(13) Uani 1 1 d . . .
O7 O 0.3515(6) 0.2515(6) 0.4379(8) 0.0241(13) Uani 1 1 d . . .
O8 O 0.1529(6) 0.2226(6) 0.6036(8) 0.0189(12) Uani 1 1 d . . .
OH1 O 0.9615(6) 0.3094(6) 0.3917(8) 0.0188(12) Uani 1 1 d D . .
OH2 O 0.0384(6) 0.8474(6) 0.1084(8) 0.0204(13) Uani 1 1 d D . .
OW1 O 0.3087(7) 0.2407(7) 0.0120(9) 0.0267(14) Uani 1 1 d D . .
OW2 O 0.6922(7) 0.4330(6) 0.4882(9) 0.0246(13) Uani 1 1 d D . .
OW3 O 0.4997(7) 0.5511(7) 0.2502(9) 0.0285(14) Uani 1 1 d D . .

OW4 O 0.5032(11) 0.1024(9) 0.2504(15) 0.059(2) Uani 1 1 d D . .
 OW5 O 0.2317(7) 0.7766(7) 0.3361(9) 0.0267(14) Uani 1 1 d D . .
 OW6 O -0.2319(7) 0.0456(6) 0.1652(9) 0.0239(13) Uani 1 1 d D . .
 HOH1 H 0.946(12) 0.380(9) 0.384(15) 0.039(8) Uiso 1 1 d D . .
 HOH2 H 0.036(12) 0.927(7) 0.122(15) 0.039(8) Uiso 1 1 d D . .
 H1A H 0.311(12) 0.277(11) -0.091(8) 0.039(8) Uiso 1 1 d D . .
 H1B H 0.250(10) 0.250(12) 0.057(13) 0.039(8) Uiso 1 1 d D . .
 H2A H 0.677(11) 0.472(11) 0.577(11) 0.039(8) Uiso 1 1 d D . .
 H2B H 0.768(7) 0.490(9) 0.459(14) 0.039(8) Uiso 1 1 d D . .
 H3A H 0.554(9) 0.624(8) 0.329(11) 0.039(8) Uiso 1 1 d D . .
 H3B H 0.426(7) 0.507(10) 0.295(14) 0.039(8) Uiso 1 1 d D . .
 H4A H 0.492(12) 0.111(12) 0.140(6) 0.039(8) Uiso 1 1 d D . .
 H4B H 0.429(8) 0.038(10) 0.280(14) 0.039(8) Uiso 1 1 d D . .
 H5A H 0.213(12) 0.736(11) 0.229(7) 0.039(8) Uiso 1 1 d D . .
 H5B H 0.242(12) 0.714(10) 0.400(11) 0.039(8) Uiso 1 1 d D . .
 H6A H -0.195(12) 0.029(11) 0.260(8) 0.039(8) Uiso 1 1 d D . .
 H6B H -0.245(12) -0.027(9) 0.097(11) 0.039(8) Uiso 1 1 d D . .

loop_

_atom_site_aniso_label
 _atom_site_aniso_U_11
 _atom_site_aniso_U_22
 _atom_site_aniso_U_33
 _atom_site_aniso_U_23
 _atom_site_aniso_U_13
 _atom_site_aniso_U_12

Mn1 0.0147(6) 0.0164(6) 0.0235(7) -0.0006(5) 0.0010(4) 0.0085(5)
 Fe1 0.0128(7) 0.0091(6) 0.0141(8) -0.0031(4) -0.0037(5) 0.0077(5)
 Al1 0.0128(7) 0.0091(6) 0.0141(8) -0.0031(4) -0.0037(5) 0.0077(5)
 Fe2 0.0147(7) 0.0084(6) 0.0162(8) -0.0039(5) -0.0038(5) 0.0079(5)
 Al2 0.0147(7) 0.0084(6) 0.0162(8) -0.0039(5) -0.0038(5) 0.0079(5)
 P1 0.0124(9) 0.0082(8) 0.0169(11) -0.0021(7) -0.0012(7) 0.0062(7)
 P2 0.0130(10) 0.0097(9) 0.0162(12) -0.0013(7) -0.0032(7) 0.0073(7)
 O1 0.016(3) 0.035(3) 0.020(3) 0.000(2) 0.000(2) 0.009(3)
 O2 0.031(3) 0.020(3) 0.021(3) -0.007(2) -0.010(2) 0.019(3)
 O3 0.021(3) 0.015(2) 0.016(3) -0.002(2) 0.000(2) 0.012(2)
 O4 0.024(3) 0.015(3) 0.015(3) 0.001(2) -0.003(2) 0.010(2)
 O5 0.014(3) 0.015(2) 0.019(3) -0.002(2) -0.005(2) 0.009(2)
 O6 0.029(3) 0.019(3) 0.019(3) 0.001(2) -0.005(2) 0.019(2)
 O7 0.016(3) 0.029(3) 0.020(3) -0.004(2) -0.001(2) 0.006(3)
 O8 0.012(3) 0.017(3) 0.025(3) -0.004(2) -0.004(2) 0.007(2)
 OH1 0.025(3) 0.019(3) 0.020(3) -0.003(2) -0.004(2) 0.018(2)
 OH2 0.029(3) 0.010(2) 0.023(3) -0.005(2) -0.006(2) 0.013(2)
 OW1 0.026(3) 0.030(3) 0.030(4) -0.004(3) 0.001(3) 0.020(3)
 OW2 0.021(3) 0.018(3) 0.030(4) -0.001(2) 0.000(3) 0.007(2)
 OW3 0.035(4) 0.020(3) 0.028(4) -0.005(3) -0.007(3) 0.014(3)
 OW4 0.068(6) 0.028(4) 0.087(7) 0.000(4) 0.007(5) 0.029(4)
 OW5 0.030(3) 0.030(3) 0.028(4) -0.003(3) -0.002(3) 0.022(3)
 OW6 0.028(3) 0.018(3) 0.022(4) -0.003(2) -0.005(3) 0.012(3)

_geom_special_details

;

All esds (except the esd in the dihedral angle between two l.s. planes)
 are estimated using the full covariance matrix. The cell esds are taken
 into account individually in the estimation of esds in distances, angles
 and torsion angles; correlations between esds in cell parameters are only
 used when they are defined by crystal symmetry. An approximate (isotropic)
 treatment of cell esds is used for estimating esds involving l.s. planes.
;

loop_

_geom_bond_atom_site_label_1
_geom_bond_atom_site_label_2
_geom_bond_distance
_geom_bond_site_symmetry_2
_geom_bond_publ_flag
Mn1 O1 2.049(6) . ?
Mn1 O7 2.071(6) . ?
Mn1 OW3 2.185(6) . ?
Mn1 OW1 2.211(6) . ?
Mn1 OW2 2.219(6) . ?
Mn1 OW4 2.240(7) . ?
Fe1 O4 1.936(5) 2_766 ?
Fe1 OH2 1.964(5) 2_665 ?
Fe1 OH1 1.961(5) . ?
Fe1 O2 1.968(5) . ?
Fe1 O5 1.992(5) 1_655 ?
Fe1 OW6 2.097(6) 1_655 ?
Fe2 O8 1.951(5) 2_566 ?
Fe2 O6 1.964(5) 1_565 ?
Fe2 OH1 1.964(6) 2_666 ?
Fe2 OH2 1.963(6) . ?
Fe2 O3 1.991(5) 1_455 ?
Fe2 OW5 2.097(6) . ?
P1 O1 1.516(6) . ?
P1 O3 1.534(5) . ?
P1 O2 1.532(5) . ?
P1 O4 1.534(6) 1_554 ?
P2 O7 1.501(6) . ?
P2 O8 1.520(6) . ?
P2 O6 1.528(5) . ?
P2 O5 1.545(5) . ?
O3 Al2 1.991(5) 1_655 ?
O3 Fe2 1.991(5) 1_655 ?
O4 P1 1.534(6) 1_556 ?
O4 Fe1 1.936(5) 2_766 ?
O4 Al1 1.936(5) 2_766 ?
O5 Al1 1.992(5) 1_455 ?
O5 Fe1 1.992(5) 1_455 ?
O6 Al2 1.964(5) 1_545 ?
O6 Fe2 1.964(5) 1_545 ?
O8 Al2 1.951(5) 2_566 ?
O8 Fe2 1.951(5) 2_566 ?
OH1 Al2 1.964(6) 2_666 ?
OH1 Fe2 1.964(6) 2_666 ?
OH1 HOH1 0.79(4) . ?
OH2 Al1 1.964(5) 2_665 ?
OH2 Fe1 1.964(5) 2_665 ?
OH2 HOH2 0.80(4) . ?
OW1 H1A 0.82(4) . ?
OW1 H1B 0.77(4) . ?
OW2 H2A 0.82(4) . ?
OW2 H2B 0.78(4) . ?
OW3 H3A 0.82(4) . ?
OW3 H3B 0.79(4) . ?
OW4 H4A 0.79(4) . ?
OW4 H4B 0.79(4) . ?
OW5 H5A 0.82(4) . ?
OW5 H5B 0.81(4) . ?
OW6 Al1 2.097(6) 1_455 ?
OW6 Fe1 2.097(6) 1_455 ?
OW6 H6A 0.79(4) . ?

OW6 H6B 0.81(4) . ?

loop_
_geom_angle_atom_site_label_1
_geom_angle_atom_site_label_2
_geom_angle_atom_site_label_3
_geom_angle
_geom_angle_site_symmetry_1
_geom_angle_site_symmetry_3
_geom_angle_publ_flag
O1 Mn1 O7 179.1(2) . . ?
O1 Mn1 OW3 90.1(2) . . ?
O7 Mn1 OW3 90.8(2) . . ?
O1 Mn1 OW1 90.2(2) . . ?
O7 Mn1 OW1 89.9(2) . . ?
OW3 Mn1 OW1 88.1(2) . . ?
O1 Mn1 OW2 89.9(2) . . ?
O7 Mn1 OW2 90.1(2) . . ?
OW3 Mn1 OW2 87.9(2) . . ?
OW1 Mn1 OW2 176.0(2) . . ?
O1 Mn1 OW4 89.6(3) . . ?
O7 Mn1 OW4 89.5(3) . . ?
OW3 Mn1 OW4 179.4(3) . . ?
OW1 Mn1 OW4 92.4(3) . . ?
OW2 Mn1 OW4 91.5(3) . . ?
O4 Fe1 OH2 89.8(2) 2_766 2_665 ?
O4 Fe1 OH1 96.7(2) 2_766 . ?
OH2 Fe1 OH1 173.1(2) 2_665 . ?
O4 Fe1 O2 91.7(2) 2_766 . ?
OH2 Fe1 O2 90.8(2) 2_665 . ?
OH1 Fe1 O2 91.4(2) . . ?
O4 Fe1 O5 90.8(2) 2_766 1_655 ?
OH2 Fe1 O5 87.6(2) 2_665 1_655 ?
OH1 Fe1 O5 89.9(2) . 1_655 ?
O2 Fe1 O5 177.0(2) . 1_655 ?
O4 Fe1 OW6 177.6(2) 2_766 1_655 ?
OH2 Fe1 OW6 89.4(2) 2_665 1_655 ?
OH1 Fe1 OW6 84.2(2) . 1_655 ?
O2 Fe1 OW6 86.1(2) . 1_655 ?
O5 Fe1 OW6 91.4(2) 1_655 1_655 ?
O8 Fe2 O6 91.7(2) 2_566 1_565 ?
O8 Fe2 OH1 89.6(2) 2_566 2_666 ?
O6 Fe2 OH1 91.2(2) 1_565 2_666 ?
O8 Fe2 OH2 97.2(2) 2_566 . ?
O6 Fe2 OH2 91.1(2) 1_565 . ?
OH1 Fe2 OH2 172.8(2) 2_666 . ?
O8 Fe2 O3 90.6(2) 2_566 1_455 ?
O6 Fe2 O3 177.5(2) 1_565 1_455 ?
OH1 Fe2 O3 87.9(2) 2_666 1_455 ?
OH2 Fe2 O3 89.6(2) . 1_455 ?
O8 Fe2 OW5 177.4(2) 2_566 . ?
O6 Fe2 OW5 86.2(2) 1_565 . ?
OH1 Fe2 OW5 89.0(2) 2_666 . ?
OH2 Fe2 OW5 84.3(3) . . ?
O3 Fe2 OW5 91.5(2) 1_455 . ?
O1 P1 O3 110.9(3) . . ?
O1 P1 O2 108.4(3) . . ?
O3 P1 O2 108.7(3) . . ?
O1 P1 O4 107.5(3) . 1_554 ?
O3 P1 O4 111.9(3) . 1_554 ?
O2 P1 O4 109.4(3) . 1_554 ?

07 P2 O8 106.6(3) . . ?
07 P2 O6 108.5(3) . . ?
08 P2 O6 110.0(3) . . ?
07 P2 O5 111.3(3) . . ?
08 P2 O5 112.0(3) . . ?
06 P2 O5 108.3(3) . . ?
P1 O1 Mn1 140.8(4) . . ?
P1 O2 Fe1 138.8(3) . . ?
P1 O3 Al2 139.2(3) . 1_655 ?
P1 O3 Fe2 139.2(3) . 1_655 ?
Al2 O3 Fe2 0.00(9) 1_655 1_655 ?
P1 O4 Fe1 131.4(3) 1_556 2_766 ?
P1 O4 Al1 131.4(3) 1_556 2_766 ?
Fe1 O4 Al1 0.00(10) 2_766 2_766 ?
P2 O5 Al1 138.7(3) . 1_455 ?
P2 O5 Fe1 138.7(3) . 1_455 ?
Al1 O5 Fe1 0.00(5) 1_455 1_455 ?
P2 O6 Al2 139.7(3) . 1_545 ?
P2 O6 Fe2 139.7(3) . 1_545 ?
Al2 O6 Fe2 0.00(11) 1_545 1_545 ?
P2 O7 Mn1 140.5(4) . . ?
P2 O8 Al2 131.0(3) . 2_566 ?
P2 O8 Fe2 131.0(3) . 2_566 ?
Al2 O8 Fe2 0.000(10) 2_566 2_566 ?
Fe1 OH1 Al2 133.4(3) . 2_666 ?
Fe1 OH1 Fe2 133.4(3) . 2_666 ?
Al2 OH1 Fe2 0.00(7) 2_666 2_666 ?
Fe1 OH1 HOH1 108(8) . . ?
Al2 OH1 HOH1 118(8) 2_666 . ?
Fe2 OH1 HOH1 118(8) 2_666 . ?
Al1 OH2 Fe1 0.00(7) 2_665 2_665 ?
Al1 OH2 Fe2 133.6(3) 2_665 . ?
Fe1 OH2 Fe2 133.6(3) 2_665 . ?
Al1 OH2 HOH2 123(7) 2_665 . ?
Fe1 OH2 HOH2 123(7) 2_665 . ?
Fe2 OH2 HOH2 103(7) . . ?
Mn1 OW1 H1A 125(8) . . ?
Mn1 OW1 H1B 101(8) . . ?
H1A OW1 H1B 107(8) . . ?
Mn1 OW2 H2A 115(7) . . ?
Mn1 OW2 H2B 114(8) . . ?
H2A OW2 H2B 111(8) . . ?
Mn1 OW3 H3A 124(7) . . ?
Mn1 OW3 H3B 85(8) . . ?
H3A OW3 H3B 102(8) . . ?
Mn1 OW4 H4A 80(8) . . ?
Mn1 OW4 H4B 109(8) . . ?
H4A OW4 H4B 112(9) . . ?
Fe2 OW5 H5A 102(7) . . ?
Fe2 OW5 H5B 110(8) . . ?
H5A OW5 H5B 102(7) . . ?
Al1 OW6 Fe1 0.00(13) 1_455 1_455 ?
Al1 OW6 H6A 92(8) 1_455 . ?
Fe1 OW6 H6A 92(8) 1_455 . ?
Al1 OW6 H6B 111(8) 1_455 . ?
Fe1 OW6 H6B 111(8) 1_455 . ?
H6A OW6 H6B 100(7) . . ?

loop_
_geom_hbond_atom_site_label_D
_geom_hbond_atom_site_label_H

_geom_hbond_atom_site_label_A
_geom_hbond_distance_DH
_geom_hbond_distance_HA
_geom_hbond_distance_DA
_geom_hbond_angle_DHA
_geom_hbond_site_symmetry_A

OH1 HOH1 O3 0.79(4) 2.14(6) 2.880(7) 156(10) .
OH2 HOH2 O5 0.80(4) 2.12(6) 2.875(7) 158(10) 1_565
OW1 H1B O5 0.77(4) 2.19(6) 2.844(9) 142(9) .
OW1 H1A OW3 0.82(4) 2.35(8) 2.992(10) 135(9) 2_665
OW2 H2B O3 0.78(4) 2.16(6) 2.846(9) 148(10) .
OW2 H2A OW3 0.82(4) 2.28(6) 2.985(10) 144(9) 2_666
OW3 H3A O7 0.82(4) 1.90(5) 2.693(8) 162(10) 2_666
OW3 H3B OW2 0.79(4) 2.35(7) 2.985(10) 138(9) 2_666
OW4 H4A O1 0.79(4) 2.64(10) 3.026(11) 112(9) .
OW5 H5A O2 0.82(4) 1.82(4) 2.636(8) 170(10) 2_665
OW5 H5B OW2 0.81(4) 1.98(5) 2.773(8) 164(11) 2_666
OW6 H6A O6 0.79(4) 1.89(5) 2.638(8) 158(10) 2_556
OW6 H6B OW1 0.81(4) 2.00(5) 2.781(8) 163(10) 2

_diffrrn_measured_fraction_theta_max 0.907
_diffrrn_reflns_theta_full 25.00
_diffrrn_measured_fraction_theta_full 0.907
_refine_diff_density_max 1.058
_refine_diff_density_min -0.678
_refine_diff_density_rms 0.171